TÜBİTAK

Turkish Journal of Earth Sciences

http://journals.tubitak.gov.tr/earth/

Research Article

Turkish J Earth Sci
(2020) 29: 684-695

doi:10.3906/yer-2001-15

Joint modeling of Rayleigh wave dispersion and H/V spectral ratio using Pareto-based multiobjective particle swarm optimization

Ersin BÜYÜK[1,*], Ekrem ZOR[2], Abdullah KARAMAN[2]

[1]İstanbul Technical University, Department of Geophysics, İstanbul, Turkey

[2]TÜBİTAK Marmara Research Center, Earth and Marine Sciences Institute, Kocaeli, Turkey

Received: 10.01.2020 • **Accepted/Published Online:** 03.04.2020 • **Final Version:** 05.05.2020

Abstract: Estimating the shear wave velocity and thickness of geologic units in a sedimentary structure is important for quantifying the local site effect caused by an earthquake. Inversion of the Rayleigh wave dispersion alone is sensitive to the absolute average shear wave velocity, while the H/V spectral ratio is sensitive to velocity contrasts. The solution of these models in a joint system using conventional inversion techniques suffers from difficulties while evaluating partial derivatives, dependencies to the initial model that is sometimes difficult to estimate, and trapping at a local minimum. Herein, a joint model using the Pareto optimality technique with multiobjective particle swarm optimization was constructed as an effective global optimization method to decrease weakness and increase performance while estimating the depths and velocities. The presented approach is a multiobjective optimization method that does not require weighting, and allows evaluations of the individual objective function separately in a joint system. This study presents 2 synthetic joint system examples to account for a gradient-type and sharp velocity contrast cases, and an application from field data obtained from the Bursa Basin in Turkey. With these examples, an automated parameter search space was demonstrated to account for the abrupt velocity changes and a number of additional key points that are essential for a reasonable optimal solution.

Key words: Particle swarm optimization, Pareto optimality, Rayleigh wave dispersion, H/V spectral ratios, earthquake, joint inversion, multiobjective optimization

1. Introduction

The local site effect causes heavy damage to settlements over sedimentary structures, regardless of the distance to the epicenter of the earthquake (Tezcan et al., 2002; Özel et al., 2002; Ergin et al., 2004; Bozdağ and Kocaoğlu, 2005). Estimating damage and mitigating risks during an earthquake is based on the shear wave velocity and thickness of the sedimentary structure that control the local site effects. For the purpose, fast and noninvasive methods based on measuring seismic noise have been popular to obtain the Rayleigh wave dispersion (RWD), and horizontal to vertical spectral ratio (HVSR) curves that are strongly related with the ellipticity of Rayleigh waves (Konno and Ohmachi, 1998; Bard, 1999; Parolai et al,. 2001; Ohrnberger et al., 2004; Wathelet et al., 2008; Özalaybey et al., 2011).

The phase velocities on the RWD curves are sensitive to the absolute average shear velocity of the material at the penetrated depth range, while HVSR curves are most sensitive to the velocity contrast with a trade-off between the depth to the contrasting interface and the average velocity above the interface. Unfortunately, the inversion of these curves separately suffers from the nonuniqueness caused by the coupled relationship between the shear wave velocity and the thickness of the sedimentary cover (Scherbaum et al., 2003). On the other hand, joint solution of the phase velocity together with ellipticity, as an additional constraint that contributes to independent information and increases the uniqueness of the common parameters (Boore and Toksöz, 1969). To overcome the nonuniqueness in the inversion process, some studies have used linearized inversion with different initial models in a multilayered scheme (Ammon et al. 1993; Herrmann 2002), joint linearized inversion (Özalaybey et al. 1997; Arai and Tokimatsu, 2005; Parolai et al., 2005; Richwalski et al., 2007), or combined inversion (Satoh et al., 2001; Scherbaum et al., 2003; Köhler et al., 2007; Zor et al., 2010). It is a well-known fact that the solution with conventional inversion techniques for this joint system suffers from difficulties while evaluating partial derivatives, dependencies to the initial model that is sometimes difficult to estimate, and trapping at a local minimum.

* Correspondence: ebuyuk@itu.edu.tr

Multiobjective global optimization methods with a probabilistic approach that has random distribution with intelligent algorithms, such as the genetic algorithm (Parolai et al., 2006; Dal Moro and Pipan, 2007; Picozzi and Albarello, 2007; Dal Moro, 2010; Boxberger et al., 2011; Akca et al., 2014; Kuo et al., 2016), and particle swarm optimization (Song et al., 2012; Peksen et al., 2014), have recently been favored to overcome the aforementioned difficulties. However, either combining the objective functions or giving subjective weighting to different objective functions may still cause a deceiving solution because sensitivities differ for RWD and HVSR curves. In this study, the Pareto optimality technique, based on Pareto dominance using particle swarm optimization, was utilized to obtain a shear wave velocity model from real and synthetic and RWD and HVSR curves obtained at the margin of the Bursa Basin in Turkey, for the purpose of investigating the performance of the joint solution. Although the Pareto optimality technique and a genetic algorithm were used for the joint inversion of RWD and HVSR curves previously (Dal Moro, 2010), the particle swarm optimization technique was used herein due to its rapid convergence (Hassan et al., 2005; Shaw and Srivastava 2007; Yuan et al., 2009; Fern and Garc, 2010; Song et al., 2012; Buyuk et al., 2017). This study presents the utility of multiobjective particle swarm optimization with the Pareto optimality technique, which produced satisfying shear wave velocity and thickness of the layers without weighting requirements, and also allowed evaluations of the individual objective function separately in a joint system. This is the first study to the authors' knowledge that utilizes multiobjective particle swarm optimization with the Pareto optimality technique for joint modeling of RWD and HVSR curves.

2. Methodology

2.1. Particle swarm optimization

Modern global optimization methods (Rao, 2009), such as the genetic algorithm (Holland, 1975), particle swarm optimization (Kennedy and Eberhart, 1995), simulated annealing (Kirkpatrick et al., 1983), and ant colony optimization (Colorni et al., 1991), have been developed over the recent decades as an alternative to conventional nonlinear inversion techniques. Among these, the particle swarm optimization method was inspired by the movements of fish or bird swarm-like colonies. Conceptually, particles representing the value of a parameter during the search denoted by each bird or fish of the swarm changes their position in the model space with a so called velocity vector (note that this is not related to the seismic wave velocity), indicating a change in the value and direction of the model parameter from the previous position to an updated one. The velocity vector is determined by the previous position, the information that is obtained from the neighboring particles, and the information shared in the swarm. In our case, the particles carrying the parameter information are earth models with shear wave velocities and layer thicknesses, and they update their new positions and the velocity vectors in the search space as:

$$V_i^{k+1} = \omega V_i^{k+1} + c_1 Y_1 (P_{best} - s_i^k) + c_2 Y_2 (g_{best} - s_i^k) \quad (1)$$

where

$$s_i^{k+1} = s_i^k + V_i^{k+1} \quad (2)$$

Here V_i^k is the velocity vector of *ith* particle at *kth* iteration; ω is the inertia weight adjusting the particle velocities to avoid excess change (Shi and Eberhart, 1998); Y_1 and Y_2 are uniformly distributed random numbers in the interval [0,1]; Y_{best} and g_{best} are the previous best values of the individual particle and the entire swarm, respectively; c_1 and c_2 are the individual learning and group learning coefficients, respectively; and s_i^k is the current position.

Learning coefficients c_1 and c_2 in Eq. (1) indicate the relative importance of the previous position of a particle to the previous position of the swarm, which are also called the acceleration coefficients of the motion of the particles (Poli et al., 2007). The higher values of c_1 (cognitive acceleration coefficient) allows the particle to move with larger deviations in the search space, while the higher values of c_2 (social acceleration coefficient) increase the convergence to the g_{best} (Tripathi et al., 2007). Kennedy (1998), and Carlisle and Dozier (2001) proposed $c_1 + c_2 \leq 4$ for as feasible searching capabilities of the system between global (more explorative) and local searches (more exploitative) in the parameter search space.

2.2. Pareto-based multiobjective particle swarm optimization

Nonunique solutions remain a persistent problem with single objective optimization in terms of the global optimization problem (Foti et al., 2009). The optimized solution in this case may exhibit equally probable nonunique solutions or conflicting solutions that may be meaningless or difficult to verify against the physical nature of the earth model. Multiobjective optimization is applied to reach a unique solution, which is basically similar to the conventional joint inversion scheme. However, unlike the conventional one, there is no need to evaluate the partial derivatives with respect to the model parameters, and an initial model in multiobjective global optimization for joint modeling. Each objective function may provide equally probable nonunique solutions independently, and finding an acceptable solution in multiobjective optimization requires overcoming the difficulty of how to evaluate, combine, and adjust their weight for the solution.

Pareto-based multiobjective particle swarm optimization requires obtaining the solutions for each objective function separately, as conceptually illustrated

in Figure 1. The horizontal and vertical axes are the misfit values (a) between the observed (y_i^{obs}) and calculated (y_i^{cal}) values from each objective function at a given search step, calculated using:

$$\alpha = \left[\frac{1}{n}\sum_{i=1}^{n}\left(y_i^{obs} - y_i^{cal}\right)^2\right]^{1/2} \quad (3)$$

where n is the number of observations. Dominant solutions referred to as the Pareto front (or leader) are constructed from the (a_1, a_2) pair obtained individually from each objective function at each iteration (Figure 1). The Pareto optimum solution nearest the origin is the solution among the Pareto front.

Figure 2 illustrates a flow chart for the implementation of the Pareto-based multiobjective particle swarm optimization algorithm. The particle positions correspond to the positions of a randomly selected shear wave velocity model in the parameter search space; the misfit values are computed for each particle position in the objective function space using Eq. (3). Determining the Pareto front solutions, as explained in Figure 1, and selecting a leader among these solutions are essential to reach the final solution. For the purpose, the objective function space is divided into cells with adaptive gridding for the successive iterations to account for the new distribution of the Pareto front. This gridded space is analyzed to find grids with Pareto front solutions, and the leader among them is selected using a roulette wheel selection scheme (Coello Coello and Reyes-Sierra, 2006; Rao, 2009). The velocity vector and position for all of the particles are updated using Eqs. (1) and (2). Each particle position is updated only if the new position produces a better solution than the previous one. Having the particle position updated, the Pareto front solutions and leader selection continue until the last iteration.

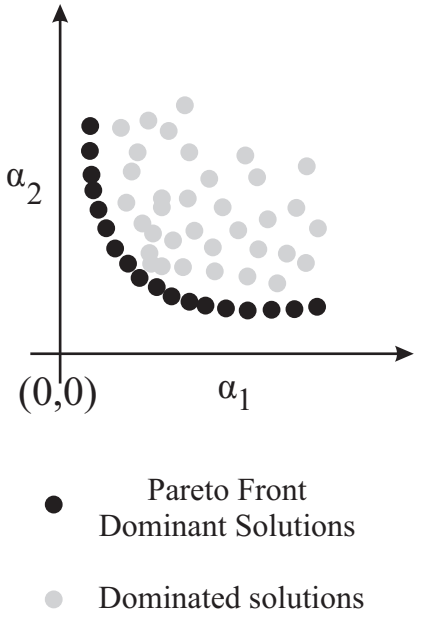

Figure 1. Conceptual representation of the Pareto front distribution. Here, a_1 and a_2 are the misfits obtained from individual objective functions. The black and light dots are the dominant solutions conforming to the Pareto Front and dominated solutions, respectively.

3. Synthetic data set and model construction

Figure 3 illustrates the synthetic RWD and HVSR (ellipticity) curves that were generated from a homogeneous, isotropic, and plane-layered medium that had shear wave velocities that smoothly increased with depth (henceforth referred to as SM-1), and a prominent shear wave velocity contrast at the third interface (henceforth referred to as SM-2). P-wave velocities in these models were calculated with an exponentially decaying v_p/v_s ratio, starting from 4 at the top layer and going up to 1.7 at the bottom, as typically observed in sedimentary basins (Zor et al., 2010). The approach presented by Tezcan et al. (2006) was used to set the model density values using the P-wave velocities. The synthetic dispersion and ellipticity curves for the fundamental mode were generated by using the open-source SESARRAY software package developed during the SESAME European Project[1]. Although higher modes, if observed and properly identified in field data applications, are preferred, since they reduce the nonuniqueness in dispersion modeling (Dal Moro, 2010; Zor et al., 2010), only fundamental mode was generated in the synthetic examples of the RWD and HVSR curves as the focus is the Pareto-based multiobjective particle swarm optimization in this study. Moreover, the phase velocities in the RWD curves were used with a frequency greater than 1.8 Hz to represent the resolution limit or sediment filtering effect (Fäh et al., 2001; Scherbaum et al., 2003).

4. Field data and site description

The microtremor data using active-passive array, and single-station measurements were acquired at the margin of the Bursa Basin at the T051 location marked in Figure 4, where the geology map was simplified based on the ages of the geologic units. Quaternary sediments at the top overlay the Miocene and Pliocene units that are underlain by a Mesozoic and Paleozoic base at the site. The central Quaternary Basin extends approximately 10 km in the NS and 25 km in the EW direction, with an average elevation of approximately 100 m.

[1] Bard PY (2002). Extracting information from ambient seismic noise: the SESAME project (Site EffectS assessment using AMbient Excitations). European Project EVG1-CT-2000-00026 SESAME, http://sesame-fp5.obs.ujf-grenoble.fr

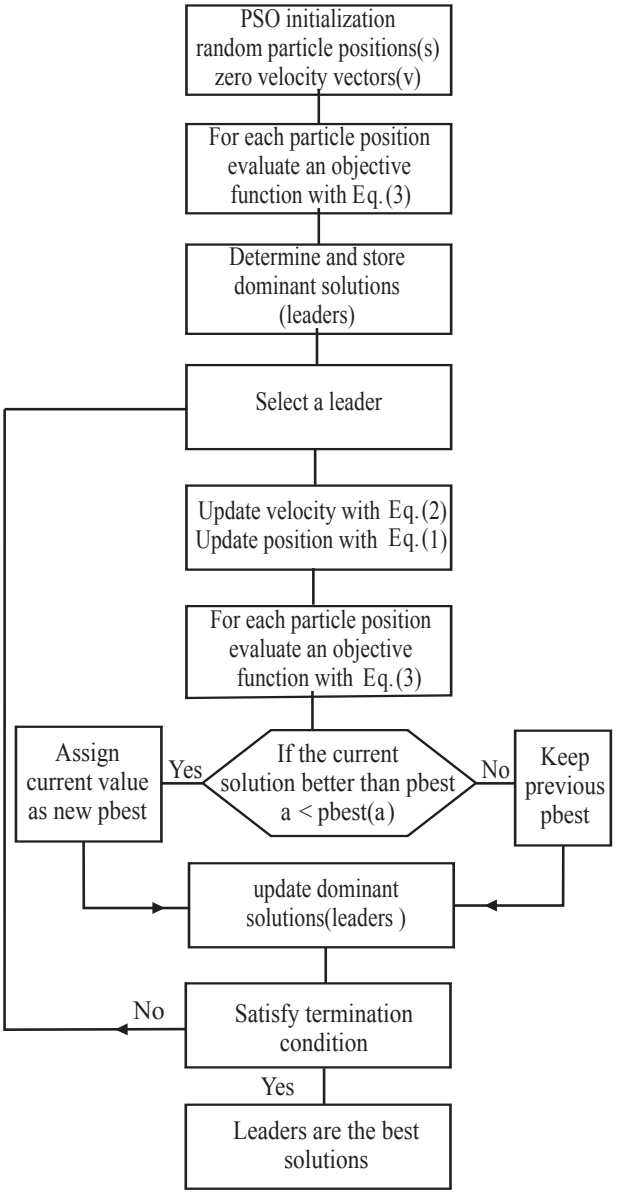

Figure 2. Flowchart of the multiobjective particle swarm optimization.

The seismologic data that were used to obtain the RWD and HVSR curves were collected during field studies for the project entitled "Site Classification and Seismic Hazard Assessment of Bursa City"[2], and were provided by the Earth and Marine Sciences Institute at the Marmara Research Center of Turkish Scientific and Technical Research Council (TÜBİTAK). The microtremor array and single-station data were collected at 500 samples per second, as described by (Zor et al., 2010) using RefTek Texan-125 single-channel recorders (Plano, TX, USA) mated with 4.5-Hz vertical-component sensors in the active and passive array measurements. The internal clocks of the independent Texan-125 recorders were synchronized using a GPS antenna prior to the array measurements being taken. To perform the single-station microtremor measurements at the center of the array, a 3-component L43C seismometer was deployed that had a natural frequency of 1 Hz, with a RefTek DAS 130 recorder equipped with a GPS antenna that was also operated at 500 samples per second.

Passive array measurements over 4 semicircles around a central station, each with 6 seismometers deployed at 30° azimuthal increments with radii of 20, 50, 90, and 120 m, and 25 in total, were performed to collect ambient noise data. Active array data were acquired over a 120-m-long linear array with a station interval of 5 m, using a sledge hammer as a seismic source; noise data were collected for at least 1 h prior to the active array measurement. Passive and active array and single station data were processed to obtain the RWD curve using the multichannel analysis of the surface wave, frequency-wavenumber, and modified spatial autocorrelation method, and the HVSR curve using the Nakamura method with the open-source SESARRAY software package. Zor et al. (2010) provided a lengthy discussion about how to pick the phase velocities to obtain the RWD curve.

5. Results and discussion

5.1. Selecting the parameter search space and multiobjective particle swarm optimization parameters

Although particle swarm optimization does not require an initial model, as is the case of conventional inversion techniques, defining a parameter search space that bounds the optimized solution for each parameter is important for reasonable solution and efficiency. Figure 5 illustrates the 5-layered reference velocity models for SM-1 and SM-2 obtained from the RWD curve following the approach described by Zor et al. (2010), based on the approximations of Park et al. (1999) and Stokoe et al. (1994). It is important to emphasize that the reference velocity model generated from the RWD curve in Figure 5a is reasonably close to the true model for SM-1, as opposed to Figure 5b, which exhibits insensitive response to the sharp velocity contrast for SM-2. Insensitivity to the velocity contrast occurs because the phase velocity in the RWD curve is sensitive to the absolute average shear velocity at the depth range associated with the respective wavelength. Figure 5 also illustrates the parameter search space for velocities and the thicknesses that were assumed as ±35% about the reference model. An exception was necessary for the upper

[2] Zor E, Özalaybey S (2013) Site Classification in Bursa Province, Turkey using microtremor array measurements, Final report, Project Code: 5117701, TÜBİTAK MRC. (http://ydbe.mam.tubitak.gov.tr/tr/haber/zemin-siniflamasi ve sismik tehlike-degerlendirme-projesi).

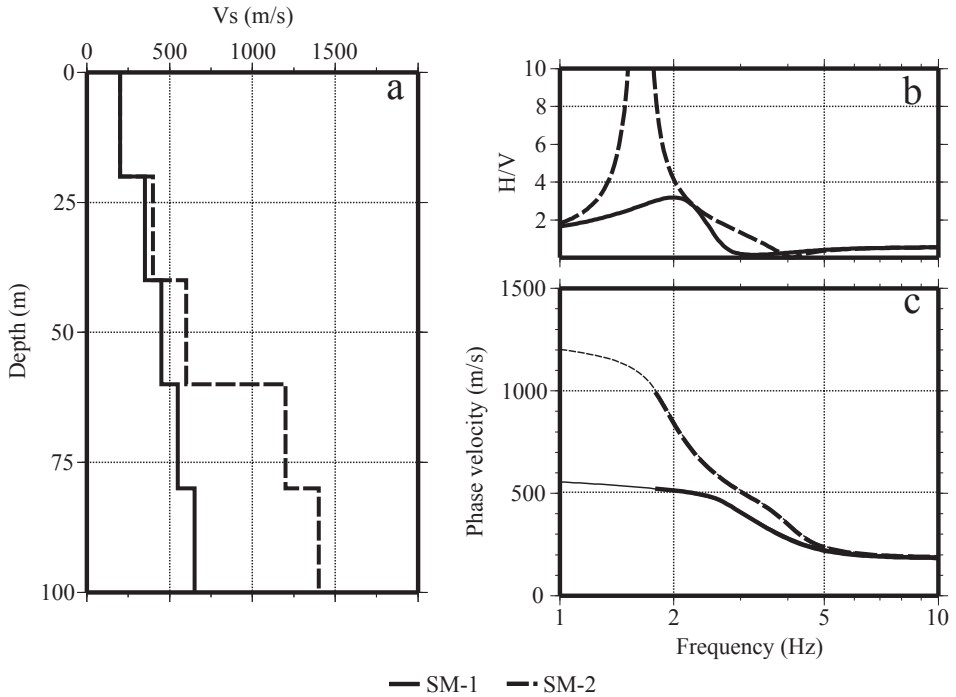

Figure 3. The velocity-depth functions (a) that are used to generate the HVSR or ellipticity curves (b), and the RWD curves (c) for SM-1 and SM-2.

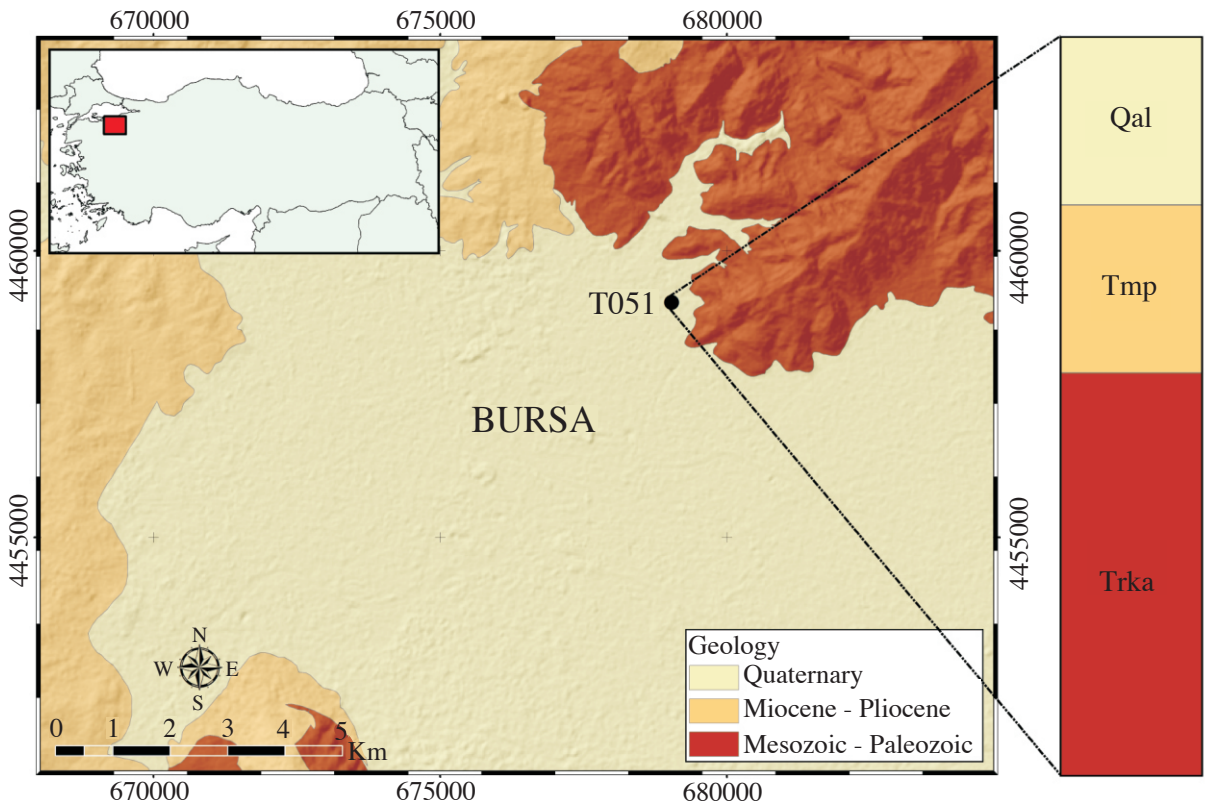

Figure 4. A simplified geological map of the Bursa Basin, and a simplified vertical column indicating the geological units at the study site labeled T051, where the array measurements were performed.

Parameter Search Space	
Thickness Interval (m)	Vs Interval (m/s)
11 - 23	135 - 415
11 - 23	215 - 660
11 - 23	287 - 884
11 - 23	328 - 1008
11 - 23	354 - 1089

Parameter Search Space	
Thickness Interval (m)	Vs Interval (m/s)
11 - 23	135 - 415
11 - 23	312 - 960
11 - 23	394 - 1214
11 - 23	490 - 1506
11 - 23	561 - 1726

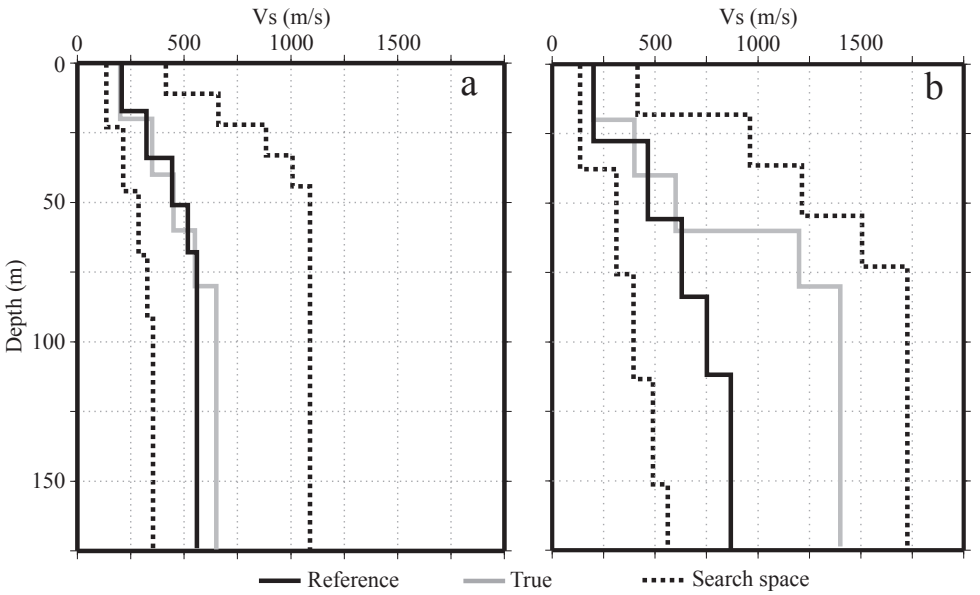

Figure 5. The true model, reference velocity model, and parameter search space for SM-1 (a) and SM-2 (b), each with numerical values of the search spaces tabulated on the top.

velocity bound, since +35% of the reference model fell too short to cover the velocities of the sharp contrast when compared with the true model for SM-2, as in Figure 5b. Therefore, the upper velocity bounds for both models were assigned to be twice the layer velocities of the reference model that would be expected to produce a broad enough search space for SM-2 than that required for SM-1. A wide enough search space ensures covering the excess velocities and abrupt interfaces that may present in the data. Figure 6 illustrates the 10-layered reference model and parameter search space obtained from the field data using the same approach. It is important to emphasize the importance of the synthetic examples, as SM-2 guided us using a broad enough search space for the field data application.

The number of iterations was set to 200 for SM-1 and SM-2, and 1000 for the field data application, which was assumed to be large enough to determine the stability of the PSO algorithm and also obtain all possible solutions. The number of particles was set to 100 for SM-1 and SM-2 (thicknesses and velocities for 5 layers), and 200 for the field data application (thicknesses and velocities for 10 layers), which was chosen to be 10-fold the number of model parameters, as suggested by Pace et al. (2019). To keep the searching capability of the system under control and prevent explosion of the swarm, learning coefficients of 2.05, constriction factor of 0.729, and grid numbers of 30 were used in each objective function, as suggested by Coello Coello and Reyes-Sierra (2006).

5.2. Synthetic models

Figure 7 illustrates the results of the joint solution for the synthetic RWD and HVSR curves generated from SM-1. The assigned parameter search space in Figure 7a, grid numbers, and number of iterations appeared to successfully reproduce the true model illustrated in Figures 7b and 7c. As pointed out by Dal Moro (2010), the symmetric distribution of the Pareto front in Figure 7d (rescaled in Figure 7e) indicated that particles clustered towards the Pareto front with a balanced motion of the particles in the adopted search space was an indicator of a properly accomplished solution. The adopted search space for the true model appeared to create a well-balanced search space for the gradient-type velocity model. The Pareto fronts extracted from the last iteration in Figure 7e were very close to each other, which was an indication of the convergence to the true model.

Figure 8 illustrates the results for SM-2, which account for the sharp velocity contrast. Figures 8b and 8c show that the synthetically generated observations matched

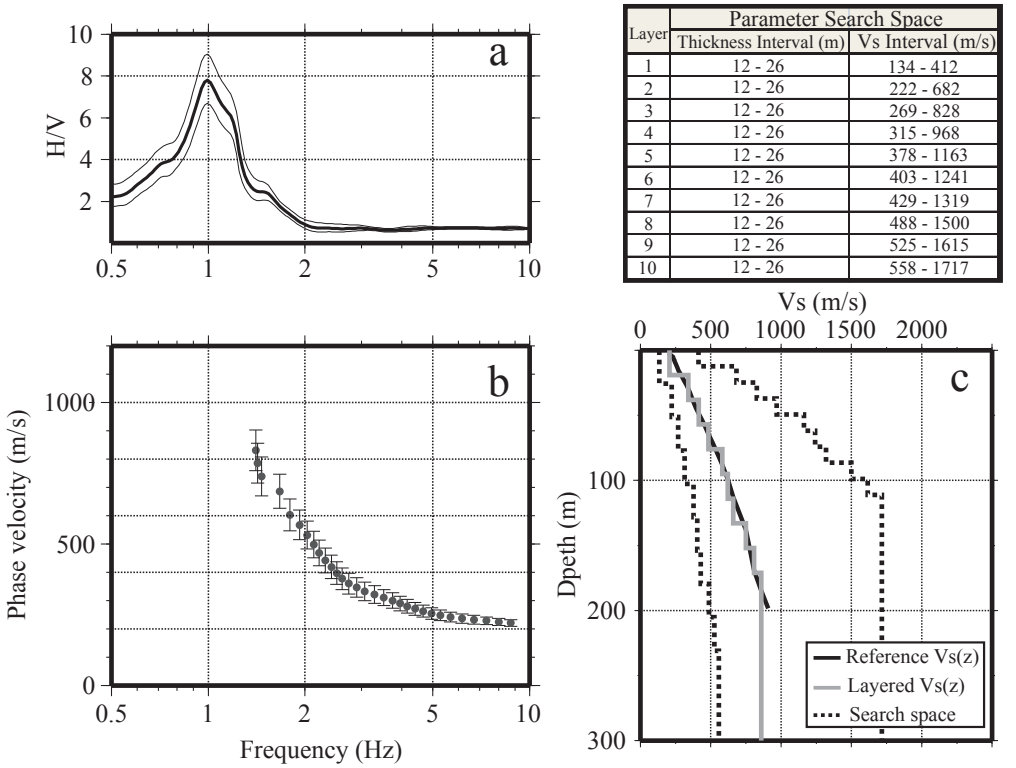

Layer	Parameter Search Space	
	Thickness Interval (m)	Vs Interval (m/s)
1	12 - 26	134 - 412
2	12 - 26	222 - 682
3	12 - 26	269 - 828
4	12 - 26	315 - 968
5	12 - 26	378 - 1163
6	12 - 26	403 - 1241
7	12 - 26	429 - 1319
8	12 - 26	488 - 1500
9	12 - 26	525 - 1615
10	12 - 26	558 - 1717

Figure 6. The HVSR (a) and RWD (b) curves with standard deviations at the location of T051, and the reference velocity model (c) with the search space. The search space intervals for the velocities and the layer thicknesses are tabulated at the top right.

perfectly with the model output and that our choice for the search space and the other settings were reasonable. Figures 8d and 8e show that particles clustered towards the Pareto front solutions fit successfully with the distribution slanted toward the RWD-axis. As common knowledge in Pareto-based multiobjective particle swarm optimization, particles fronting towards the RWD-axis correspond to good solutions with a small misfit between the observed and calculated HVSR curves, while particles close to the HVSR-axis are related with a good RWD match in a similar way. Distribution of this type, as in Figure 8d, indicated nonunique solution. This suggested that there were more solutions satisfying the HVSR objective function than were equally compared to the RWD objective function for the case having a sharp peak in the HVSR curve when compared to SM-1 in Figure 7d. Hence, the nonsymmetry of the Pareto distribution was not only related to a properly accomplished inversion (Dal Moro, 2008), but also to the characteristic of the HVSR inversion in the case of having sharp velocity contrast. Obviously, several alternative models can be considered as a final model, when a single objective function is used based on the HVSR misfit with its several local minima. Moreover, the global minimum converges successfully at higher iterations with multiobjective particle swarm optimization. As illustrated in Figure 8, the curves generated from the Pareto front models obtained in the last iteration fit well with the observed curves and provide identical models.

5.3. Field data from the Bursa Basin

Figure 9 illustrates results from the Bursa Basin, in which the respective parameter search space was constrained using the experience gained, especially from the synthetic model, SM-2. The Pareto distribution of the particles obtained from the last iteration in Figure 9a exhibits the nonsymmetry slanted over the RWD axis, indicating nonunique solutions. Figures 9b and 9c compare and contrast the reproduced and observed RWD and HSVR curves, labeled A, B, and C, using the velocity models in Figure 9d with the same labels over the Pareto front. The misfits for these velocity models were reasonably close to each other, as tabulated in Table, where the best was the Pareto optimum solution marked as A, with a misfit value of 1.33 for the RWD curve and 0.068 for the HVSR curve. Although the presented neighboring solutions, B and C, produced a fit that was very close to the solution that was presented as the best, a slight mismatch appears to be visible at higher and lower frequencies in the RWD curve, and higher frequencies in the HVSR curve. On the

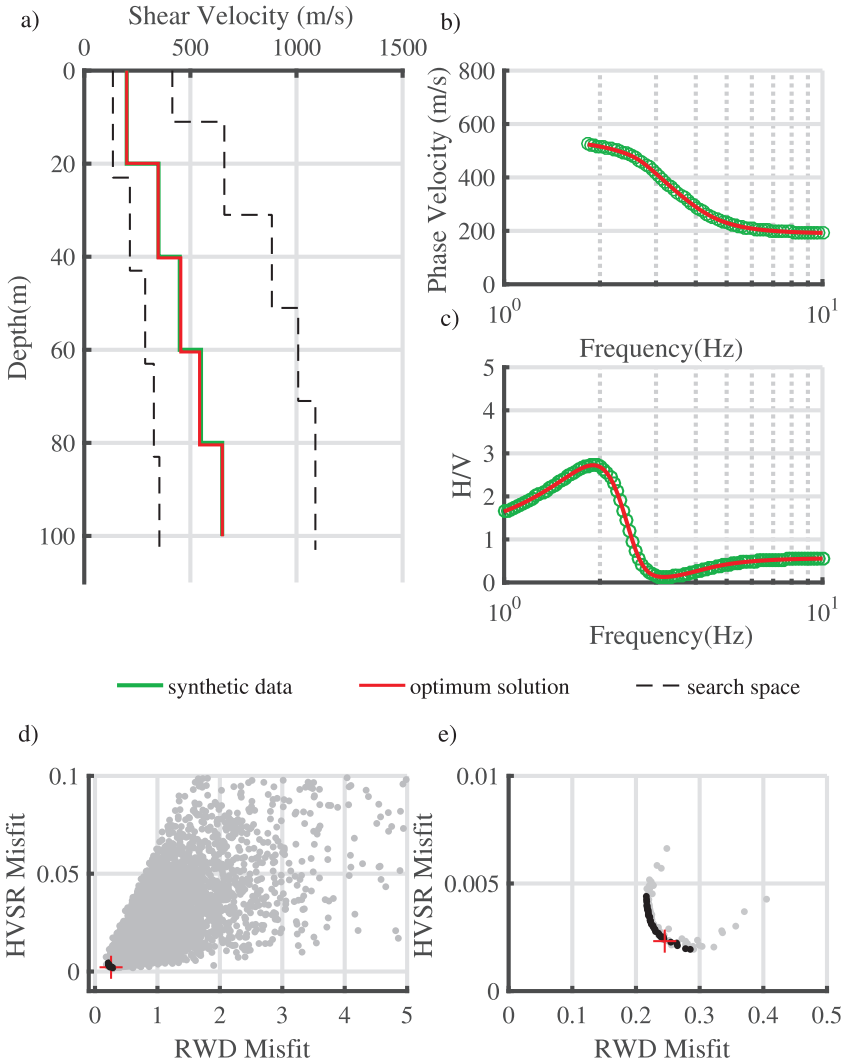

Figure 7. Results for SM-1. Shear wave velocity-depth model obtained from the Pareto optimum particle and the parameter search space (a); the fit between the observed and calculated RWD (b), and HVSR and Rayleigh wave ellipticity curves (c); the Pareto optimum solution marked as + and Pareto front (dark dots) with the Pareto distribution (light dots) for all iterations (d); and the Pareto optimum solution (+) with Pareto front at the last iteration (e).

other hand, the HVSR objective function alone appeared to provide pronounced velocity contrasts, because the shape of the HVSR curve was sensitivity to the velocity contrasts of the velocity-depth model. Therefore, utility of the Pareto-based multiobjective function provided a better constrained shear wave velocity model that was capable of reproducing the observed data set.

The final velocity model, marked as A in Figure 9d, appeared to represent the geology at the T051 location in Figure 4, where the geologic units consisted of, from the top to the bottom, Quaternary alluvium deposit, Miocene and Pliocene sediments, and Mesozoic and Paleozoic base. Two distinct velocity contrasts, at depths of 75 m and 175 m, appeared to be consistent with the 3-layered simplified column of the geological units from the surface geology. The top layer, which extends down to 75 m, with an average shear wave velocity of ~350 m/s, may reasonably be interpreted as a Quaternary alluvium deposit. The layer starting at 75 m and extending to 175 m, with a shear wave velocity of ~750 m/s, coincides with the Miocene and Pliocene sedimentary unit, and the half-space below 175 m, with a shear wave velocity of ~1200 m/s, is the Mesozoic and Paleozoic base.

6. Conclusion

We presented Pareto-based multiobjective particle swarm optimization applied on RWD and HVSR synthetic curves, and a sample data set obtained from the Bursa

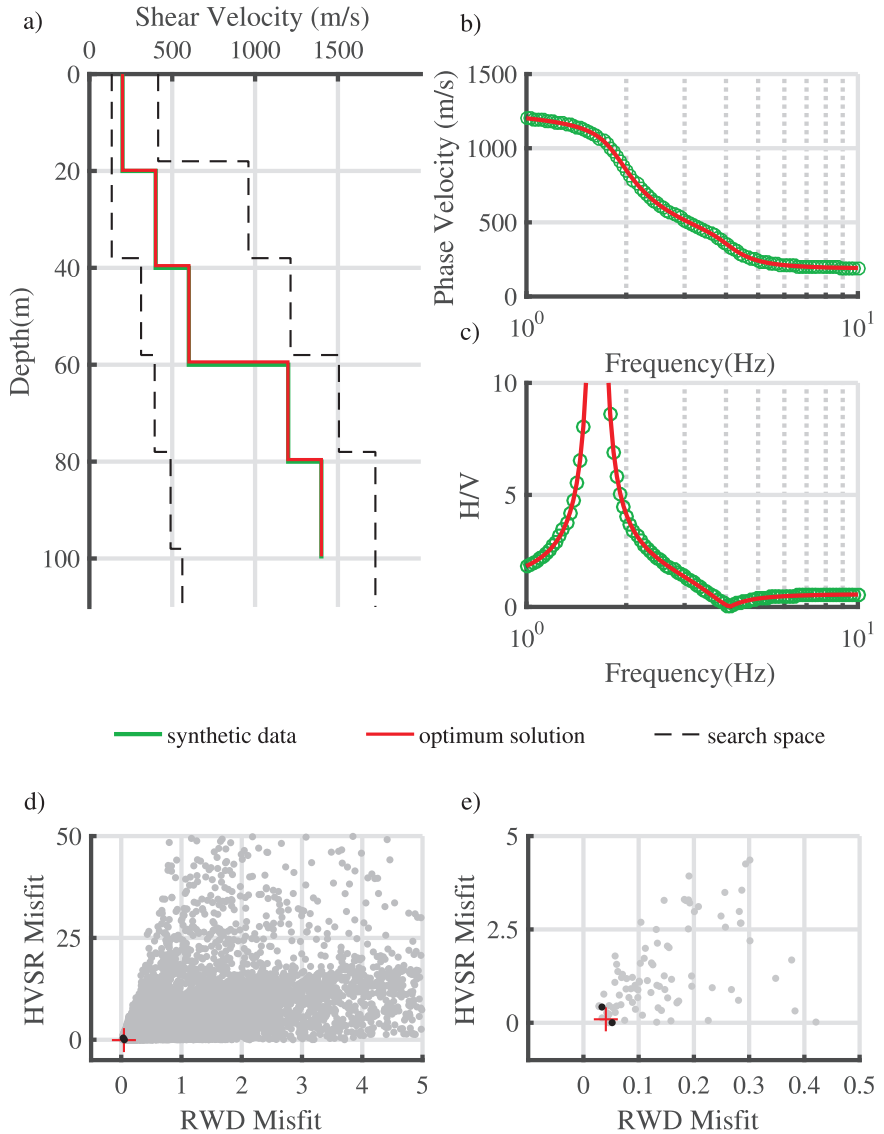

Figure 8. Results for SM-2. Shear wave velocity-depth model obtained from Pareto front particles and the parameters search space (a); the fit between the observed and calculated RWD (b), and HVSR and Rayleigh wave ellipticity curves (c); the Pareto optimum solution marked as +, and Pareto front (dark dots) with the Pareto distribution (light dots) for all iterations (d); and the Pareto optimum solution (+) with Pareto front at the last iteration (e).

Basin for the purpose of better understanding the concept of parameter search space, and the applicability of the method on the field data. There were a number of conclusions that can be drawn from this study: 1) with the utility of this method, it is possible to analyze each solution from the individual objective functions separately using the Pareto front approach; 2) setting the parameter search space broad enough for the shear wave velocity model provides convenience for an optimum solution; 3) the automated technique we developed to define the parameter search space, instead of setting a search interval manually for shear wave velocities and the depths for each layer, proved to be a useful approach; 4) it is possible to significantly reduce the computing time by limiting the parameter search space using the rough estimation from the dispersion curve; 5) in Pareto-based multiobjective particle swarm optimization, the balanced change in Pareto distribution is not only related to a well-defined parameter search space, but also to the number of trade-off solutions in each objective function; 6) nonsymmetry in Pareto distribution can be utilized to investigate the nonuniqueness of a model; and 7) the results we obtained from the field data application was satisfying, and were consistent with the vertical geological structure at the site.

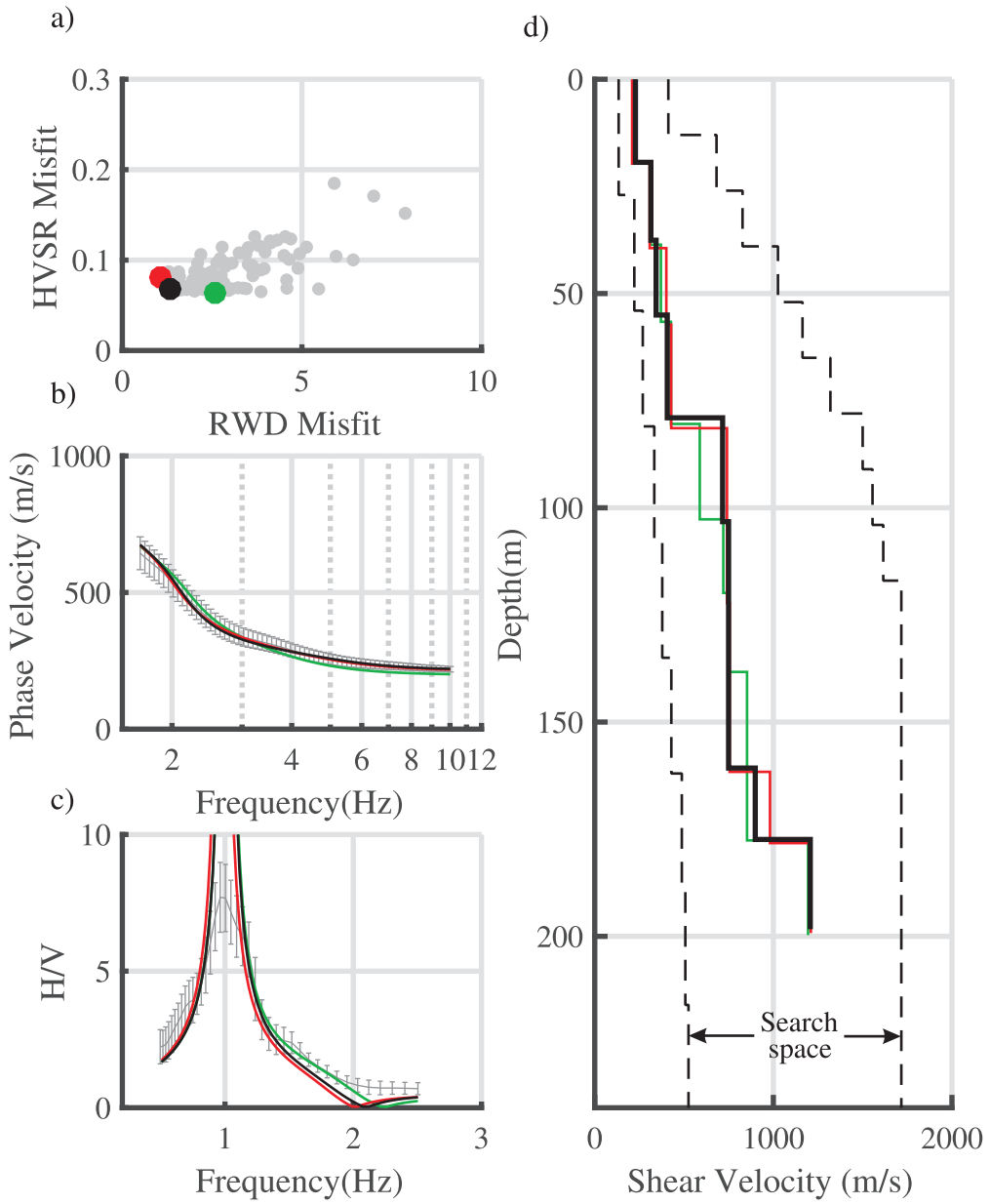

Figure 9. The results obtained for site T051. (a) Pareto distribution of the last iteration with the Pareto front particles labeled A, B, and C that are shared correspondingly in all of the following plots; (b) the fit between the observed and calculated RWD curves; (c) the fit between the observed HVSR and Rayleigh wave ellipticity; and (d) the shear wave velocity models with the one labeled A being the optimum solution.

Table. Misfit values obtained from the optimal solution A and a comparison with the neighboring misfit values of B and C in Figure 9a.

Misfit function	**A**	**B**	**C**
RWD	1.33	1.058	2.6
HVSR	0.068	0.08	0.064

Acknowledgments
We wish to thank the Earth and Marine Sciences Institute of the Marmara Research Center at The Scientific and Technological Research Council of Turkey (TÜBİTAK) for sharing the seismologic data acquired through a project entitled "Site Classification and Seismic Hazard Assessment of Bursa Province".

References

Akca I, Günther T, Müller-Petke M, Başokur AT, Yaramanci U (2014). Joint parameter estimation from magnetic resonance and vertical electric soundings using a multi-objective genetic algorithm. Geophysical Prospecting 62 (2): 364-376. doi: 10.1111/1365-2478.12082

Ammon CJ, Velasco AA, Lay T (1993). Rapid estimation of rupture directivity: Application to the 1992 Landers (MS = 7.4) and Cape Mendocino (MS = 7.2), California earthquakes. Geophysical Research Letters 20 (2): 97-100. doi: 10.1029/92GL03032

Arai H, Tokimatsu K (2005). S-wave velocity profiling by joint inversion of microtremor dispersion curve and horizontal-to-vertical (H/V) spectrum. Bulletin of the Seismological Society of America 95 (5): 1766-1778. doi: 10.1785/0120040243

Bard PY (1999). Microtremor measurement : a tool for site effect estimation? 2nd Int Symp. on the Effects of Surface Geology on Seismic Motion, Yokohama, Japan 1 (3); 1251-1279.

Boore DM, Toksöz MN (1969). Rayleigh wave particle motion and crustal structure. Bulletin of the Seismological Society of America 59 (1); 331-346.

Boxberger T, Picozzi M, Parolai S (2011). Shallow geology characterization using Rayleigh and Love wave dispersion curves derived from seismic noise array measurements. Journal of Applied Geophysics 75 (2); 345-354. doi: 10.1016/j.jappgeo.2011.06.032

Bozdağ E, Kocaoğlu AH (2005). Estimation of site amplifications from shear-wave velocity profiles in Yeşilyurt and Avcilar, Istanbul, by frequency-wavenumber analysis of microtremors. Journal of Seismology 9 (1); 87-98. doi: 10.1007/s10950-005-5271-8

Buyuk E, Zor E, Karaman A (2017). Rayleigh wave dispersion curve inversion by using particle swarm optimization and genetic algorithm. 19th EGU General Assembly, EGU2017, Proceedings from the Conference Held 23-28 April, 2017 in Vienna, Austria., p.6911, 19, 6911.

Carlisle A, Dozier G (2001). An off-the-shelf pso. In : Proceeding of Workshop on Particle Swarm Optimizaiton. Indianapolis, Purdue School of Engineering and Technology, IUPUI, Indianapolis, IN, USA.

Coello Coello CA, Reyes-Sierra M (2006). Multi-objective particle swarm optimizers: a survey of the state-of-the-art. International Journal of Computational Intelligence Research, 2(3), 1-48. doi: 10.5019/j.ijcir.2006.68

Colorni A, Dorigo M, Maniezzo V (1991). Distributed Optimization by ant colonies. Proceedings of the First European Conference on Artificial Life, 134-142.

Dal Moro G, Pipan M (2007). Joint inversion of surface wave dispersion curves and reflection travel times via multi-objective evolutionary algorithms. Journal of Applied Geophysics, 61 (1); 56-81. doi: 10.1016/j.jappgeo.2006.04.001

Dal Moro G (2010). Insights on surface wave dispersion and HVSR: Joint analysis via Pareto optimality. Journal of Applied Geophysics 72 (2); 129-140. doi: 10.1016/j.jappgeo.2010.08.004

Dal Moro G (2008). VSand VPvertical profiling via joint inversion of Rayleigh waves and refraction travel times by means of bi-objective evolutionary algorithm. Journal of Applied Geophysics 66 (1-2); 15-24. doi: 10.1016/j.jappgeo.2008.08.002

Ergin M, Aktar M, Eyidoğan H (2004). Present-Day Seismicity and Seismotectonics of the Cilician Basin: Eastern Mediterranean Region of Turkey. Bulletin of the Seismological Society of America 94 (3); 930-939. doi: 10.1785/0120020153

Fäh D, Kind F, Giardini D (2001). A theoretical investigation of average HIV ratios. Geophysical Journal International 145 (2); 535-549. doi: 10.1046/j.0956-540X.2001.01406.x

Fern JL, Garc E (2010). Appraising the Streaming-Potential Inverse Problem. Geophysics 75 (4); WA3-WA15. doi: 10.1190/1.3460842

Foti S, Comina C, Boiero D, Socco LV (2009). Non-uniqueness in surface-wave inversion and consequences on seismic site response analyses. Soil Dynamics and Earthquake Engineering, 29 (6); 982-993. doi: 10.1016/j.soildyn.2008.11.004

Hassan R, Cohanim B, Weck O de. (2005). A comparison of particle swarm optimization and the genetic algorithm. 1st AIAA Multidisciplinary Design Optimization Specialist Conference, 1-13. doi: 10.2514/6.2005-1897

Herrmann RB (2002). Computer Programs in Seismology an Overview of Synthetic Seismogram Computation. Saint Louis University, USA, Version 3.30 2002, (September).

Holland JH (1975). Adaptation in Natural and Artificial Systems: An introductory Analysis with Applications to Biology, Control and Artificial Intelligence. MIT Press, 183. doi: 10.1137/1018105

Kennedy J (1998). The behavior of particles. Evolutionary Programming VII: 7th International Conference, EP98 San Diego, California, USA, March 25–27, 1998 Proceedings doi: 10.1007/BFb0040809

Kennedy J, Eberhart R (1995). Particle swarm optimization. Neural Networks, 1995. Proceedings, IEEE International Conference On, 4, 1942–1948 vol.4. doi: 10.1109/ICNN.1995.488968

Kirkpatrick S, Gelatt CD, Vecchi MP (1983). Optimization by simulated annealing. Science, New York 220 (4598); 671-680. doi: 10.1126/science.220.4598.671

Köhler A, Ohrnberger M, Scherbaum F, Wathelet M, Cornou C (2007). Assessing the reliability of the modified three-component spatial autocorrelation technique. Geophysical Journal International 168 (2); 779-796. doi: 10.1111/j.1365-246X.2006.03253.x

Konno K, Ohmachi T (1998). Ground-motion characteristics estimated from spectral ratio between horizontal and vertical components of microtremor. Bulletin of the Seismological Society of America 88 (1); 228-241.

Kuo CH, Chen CT, Lin CM, Wen KL, Huang JY et al. (2016). S-wave velocity structure and site effect parameters derived from microtremor arrays in the Western Plain of Taiwan. Journal of Asian Earth Sciences 128; 27-41. doi: 10.1016/j.jseaes.2016.07.012

Ohrnberger M, Scherbaum F, Krüger F, Pelzing R, Reamer SK (2004). How good are shear wave velocity models obtained from inversion of ambient vibrations in the lower Rhine embayment (N.W. Germany)? Bollettino Di Geofisica Teorica Ed Applicata 45 (3); 215-232.

Özalaybey S, Savage MK, Sheehan AF, Louie JN, Brune JN (1997). Shear-wave velocity structure in the northern Basin and Range province from the combined analysis of receiver functions and surface waves. Bulletin of the Seismological Society of America 87 (1); 183-199.

Özalaybey S, Zor E, Ergintav S, Tapirdamaz MC (2011). Investigation of 3-D basin structures in the İzmit Bay area (Turkey) by single-station microtremor and gravimetric methods. Geophysical Journal International 186 (2); 883-894. doi: 10.1111/j.1365-246X.2011.05085.x

Özel O, Cranswick E, Meremonte M, Erdik M, Safak E (2002). Site effects in Avcilar, West of Istanbul, Turkey, from strong- and weak-motion data. Bulletin of the Seismological Society of America 92 (1); 499-508. doi: 10.1785/0120000827

Pace F, Santilano A, Godio A (2019). Particle swarm optimization of 2D magnetotelluric data. Geophysics 84 (3); E125-E141. doi: 10.1190/geo2018-0166.1

Park CB, Miller RD, Xia J (1999). Multichannel analysis of surface waves. Geophysics 64 (3); 800-808. doi: 10.1190/1.1444590

Parolai S, Bormann P, Milkereit C (2001). Assessment of the natural frequency of the sedimentary cover in the cologne area (Germany) using noise measurements. Journal of Earthquake Engineering 5 (4); 541-564. doi: 10.1080/13632460109350405

Parolai S, Picozzi M, Richwalski SM, Milkereit C (2005). Joint inversion of phase velocity dispersion and H/V ratio curves from seismic noise recordings using a genetic algorithm, considering higher modes. Geophysical Research Letters 32 (1); 1-4. doi: 10.1029/2004GL021115

Parolai S, Richwalski SM, Milkereit C, Fäh D (2006). S-wave velocity profiles for earthquake engineering purposes for the Cologne area (Germany). Bulletin of Earthquake Engineering 4 (1); 65-94. doi: 10.1007/s10518-005-5758-2

Peksen E, Yas T, Kiyak A (2014). 1-D DC Resistivity Modeling and Interpretation in Anisotropic Media Using Particle Swarm Optimization. Pure and Applied Geophysics 171 (9); 2371-2389. doi: 10.1007/s00024-014-0802-2

Picozzi M, Albarello D (2007). Combining genetic and linearized algorithms for a two-step joint inversion of Rayleigh wave dispersion and H/V spectral ratio curves. Geophysical Journal International 169 (1); 189-200. doi: 10.1111/j.1365-246X.2006.03282.x

Poli R, Kenney J, Blackwell T (2007). Particle swarm optimization. Swarm Intelligence 1 (1); 33-57. doi: 10.1007/s11721-007-0002-0

Rao SS (2009). Engineering Optimization: Theory and Practice: Fourth Edition. In Engineering Optimization: Theory and Practice: Fourth Edition. doi: 10.1002/9780470549124

Richwalski SM, Picozzi M, Parolai S, Milkereit C, Baliva F et al. (2007). Rayleigh wave dispersion curves from seismological and engineering-geotechnical methods: a comparison at the Bornheim test site (Germany). Journal of Geophysics and Engineering 4 (4); 349-361. doi: 10.1088/1742-2132/4/4/001

Satoh T, Kawase H, Marsushima S (2001). Estimation of S-Wave velocity structures in and around the Sendai Basin, Japan, using array records of microtremors. Bulletin of the Seismological Society of America 91 (2); 206-218. doi: 10.1785/0119990148

Scherbaum F, Hinzen KG, Ohrnberger M (2003). Determination of shallow shear wave velocity profiles in the cologne, Germany area using ambient vibrations. Geophysical Journal International 152 (3); 597-612. doi: 10.1046/j.1365-246X.2003.01856.x

Shaw R, Srivastava S (2007). Particle swarm optimization: A new tool to invert geophysical data. Geophysics 72 (2); F75. doi: 10.1190/1.2432481

Shi Y, Eberhart RC (1998). Parameter selection in particle swarm optimization. Evolutionary Programming VII; 591-600. doi: 10.1007/BFb0040810

Song X, Tang L, Lv X, Fang H, Gu H (2012). Application of particle swarm optimization to interpret Rayleigh wave dispersion curves. Journal of Applied Geophysics 84; 1-13. doi: 10.1016/j.jappgeo.2012.05.011

Stokoe KH, Wright SG, Bay JA, Roesset JM (1994). Characterization of geotechical sites by SASW method. Geophysical Characterization of Sites, 15-25.

Tezcan SS, Kaya E, Bal IE, Ozdemir Z (2002). Seismic amplification at Avcılar, Istanbul. Engineering Structures 24 (5); 661-667. doi: 10.1016/S0141-0296(02)00002-0

Tezcan SS, Keceli A, Ozdemir Z (2006). Allowable bearing capacity of shallow foundations based on shear wave velocity. Geotechnical and Geological Engineering 24 (1); 203-218. doi: 10.1007/s10706-004-1748-4

Tripathi PK, Bandyopadhyay S, Pal SK (2007). Multi-Objective Particle Swarm Optimization with time variant inertia and acceleration coefficients. Information Sciences 177 (22); 5033-5049. doi: 10.1016/j.ins.2007.06.018

Wathelet M, Jongmans D, Ohrnberger M, Bonnefoy-Claudet S (2008). Array performances for ambient vibrations on a shallow structure and consequences over Vs inversion. Journal of Seismology 12 (1); 1-19. doi: 10.1007/s10950-007-9067-x

Yuan S, Wang S, Tian N (2009). Swarm intelligence optimization and its application in geophysical data inversion. Applied Geophysics 6 (2); 166-174. doi: 10.1007/s11770-009-0018-x

Zor E, Özalaybey S, Karaaslan A, Tapirdamaz MC, Özalaybey S et al. (2010). Shear wave velocity structure of the Izmit Bay area (Turkey) estimated from active-passive array surface wave and single-station microtremor methods. Geophysical Journal International 182 (3); 1603-1618. doi: 10.1111/j.1365-246X.2010.04710.x